

1 The enhancement of neutron rich particle emission from out-of-fission-plane in Fermi energy heavy 2 ion reactions

3 Yijie Wang,^{1,*} Sheng Xiao,¹ Mengting Wan,^{2,3} Xinyue Diao,¹ Yuhao Qin,¹ Zhi Qin,¹ Dong Guo,¹ Dawei Si,¹ Boyuan Zhang,¹
4 Baiting Tian,¹ Junhuai Xu,¹ Fenhui Guan,¹ Qianghua Wu,¹ Xianglun Wei,⁴ Herun Yang,⁴ Peng Ma,⁴ Rongjiang Hu,⁴ Limin
5 Duan,⁴ Fangfang Duan,⁴ Junbing Ma,⁴ Shiwei Xu,⁴ Qiang Hu,⁴ Zhen Bai,⁴ Yanyun Yang,⁴ Jiansong Wang,^{4,5} Wenbo
6 Liu,⁶ Wanqing Su,⁶ Xiaobao Wei,⁶ Chun-Wang Ma,⁶ Xinxiang Li,^{7,8} Hongwei Wang,^{8,9} Yingxun Zhang,¹⁰ Michał
7 Warda,¹¹ Arthur Dobrowolski,¹¹ Bożena Nerlo-Pomorska,¹¹ Krzysztof Pomorski,¹¹ Li Ou,^{2,3,†} and Zhigang Xiao^{1,12,‡}

8 ¹Department of Physics, Tsinghua University, Beijing 100084, China

9 ²College of Physics and Technology, Guangxi Normal University, Guilin 541004, China

10 ³Guangxi Key Laboratory of Nuclear Physics and Technology, Guangxi Normal University, Guilin 541004, China

11 ⁴Institute of Modern Physics, Chinese Academy of Sciences, Lanzhou 730000, China

12 ⁵School of Science, Huzhou University, Huzhou, 313000, China;

13 ⁶Institute of Particle and Nuclear Physics, Henan Normal University, Xinxiang 453007, China

14 ⁷School of Nuclear Science and Technology, University of South China, Hengyang 421001, China

15 ⁸Shanghai Institute of Applied Physics, Chinese Academy of Science, Shanghai 201800, China

16 ⁹Shanghai Advanced Research Institute, Chinese Academy of Science, Shanghai 201210, China

17 ¹⁰China Institute of Atomic Energy, Beijing 102413, China

18 ¹¹Institute of Physics, Maria Curie Skłodowska University, 20-031 Lublin, Poland

19 ¹²Collaborative Innovation Center of Quantum Matter, Tsinghua University, Beijing 100084, China

20 The neutron richness of the light charged particles emitted out of the fission plane in heavy ion reactions has
21 been experimentally investigated via the production of $A = 3$ mirror nuclei in $^{86}\text{Kr} + ^{\text{n}a\text{l}}\text{Pb}$ reactions at 25 MeV/u.
22 The energy spectra and angular distributions of triton (t) and ^3He in coincidence with two fission fragments are
23 measured with the Compact Spectrometer for Heavy Ion Experiment (CSHINE). The energy spectrum of ^3He
24 is observed harder than that of triton in the fission events, in accordance with the phenomena reported as “ ^3He -
25 puzzle” in inclusive measurements. With a data driven energy spectrum peak cut scenario, it is observed that
26 the yield ratio $R(t/^3\text{He})$ increases with the angle to the fission plane, showing an enhancement of neutron rich
27 particle emission from out-of-fission-plane. A qualitative comparison with the transport model calculations
28 suggests that this observation may serve as a new probe for the nuclear symmetry energy.

29 Keywords: Heavy ion reaction, Fast fission, ^3He -puzzle, out-of-fission-plane emission, Nuclear symmetry energy

I. INTRODUCTION

31 Heavy ion reactions (HIR) provide a femtoscopic labora-
32 tory for investigating the properties of the nuclear equation
33 of state (nEoS), particularly the nuclear symmetry energy
34 $E_{\text{sym}}(\rho)$ [1–6]. The stringent constraint of $E_{\text{sym}}(\rho)$ is crucial
35 for both nuclear- and astro-physics, and draws the most at-
36 tention since the detection of the gravitational waves from the
37 neutron star merging event GW170817 [7–9]. Although great
38 progress has been made via neutron skin thicknesses[10–
39 14], nuclear charge radius[15], flow[16–18] and the detec-
40 tion of isobaric yield ratios in HIRs, like n/p [19], $t/^3\text{He}$
41 [20, 21], π^-/π^+ [22–25], K^0/K^+ [26] and Ξ^-/Ξ^0 [27], the
42 $E_{\text{sym}}(\rho)$ is still suffering a lot uncertainties [28–32], and the
43 efforts are ongoing to search novel probes to explore the ef-
44 fects of $E_{\text{sym}}(\rho)$ in HIRs [33–37].

45 The nuclear (fast)fission process is a large-amplitude col-
46 lective motion mode happening in the HIRs. The low-
47 density neutron rich neck region formed in the rupture of
48 two fission fragments provides a good condition for study-
49 ing $E_{\text{sym}}(\rho)$ and dynamic properties in isospin degree of

50 freedom (IDOF)[38–41]. The neck zone has been explored
51 to understand the mechanism of intermediate mass fragment
52 (IMF) formation [42–45], isotopic cluster emission [46–49]
53 and neutron-proton equilibration [50–54]. Because of the
54 density gradient and the isospin migration, the neck zone pro-
55 vides a beneficial environment to study the $E_{\text{sym}}(\rho)$ [52, 54].
56 For more discussions about neck zone, one can refer to the
57 review articles of heavy ion reactions from the experimental
58 [38, 39, 55] and theoretic points of view [56–60].

59 The emissions of light particles in coincidence with fission
60 fragments is a natural idea for exploring the symmetry energy
61 effect and (fast)fission properties in HIRs [40, 41]. Among
62 the probes using the light charged particles (LCPs), the yield
63 ratio of $t/^3\text{He}$, written as $R(t/^3\text{He})$, has been particularly
64 identified to probe the enriched feature of isospin dynamics
65 in HIRs. Transport model calculations demonstrate that the
66 $R(t/^3\text{He})$ at intermediate-energy HIRs depends on the stiff-
67 ness of $E_{\text{sym}}(\rho)$ [21, 61]. At high-energy HIRs, $R(t/^3\text{He})$ de-
68 pends more sensitively on the value of $E_{\text{sym}}(\rho)$ [62] and
69 the specific form of the interaction potential [25, 63], but is
70 less dependent on the slope of $E_{\text{sym}}(\rho)$ [64]. In addition,
71 $R(t/^3\text{He})$ reflects the isospin dependent nucleon density in
72 the reactions [43, 65, 66]. Experimentally, the yield ratios of
73 various mirror nucleus pairs, including the $R(t/^3\text{He})$, led to
74 the discovery of isospin fractionation [67]. It has been sug-
75 gested that more neutron-rich particles are emitted at mid-

* Corresponding author, yj-wang15@tsinghua.org.cn

† Corresponding author, liou@gxnu.edu.cn

‡ Corresponding author, xiaozg@tsinghua.edu.cn

rapidity, as inferred by the $R(t/{}^3\text{He})$, which correlates positively with the charge number of projectile-like fragments[43] but reversely with the center of mass energy [68]. Similarly, in high-energies HIR, the $R(t/{}^3\text{He})$ reflects the neutron enrichment of the emission source[43, 69, 70] and isospin mixing during the collision [71]. Recently, the $R(t/{}^3\text{He})$ has also been used to study the pick-up mechanism of pre-equilibrium light nucleus production in the pion scattering experiment [72]. Hence, the distribution of $R(t/{}^3\text{He})$ relative to the fission plane is a good prob to characterize the properties of fission process and explore the properties of symmetry energy.

Despite of the enormous progress of the studies on the triton (t) and ${}^3\text{He}$ emission, some questions remain unclear and require further studies. For example, when considering the spectra of ${}^3\text{He}$, there is an anomalous phenomenon that the yield of high energy ${}^3\text{He}$ is relatively larger, compared to that of triton [73–77] or ${}^4\text{He}$ [73, 75–78]. This phenomenon has been called “ ${}^3\text{He}$ -puzzle” [73, 74, 77]. While the energy spectra are suffering “ ${}^3\text{He}$ -puzzle”, the yield ratio of triton and ${}^3\text{He}$ is sensitive to the neutron-to-proton ratio (N/Z) of the emitting system [53, 70, 79, 80]. The excitation function of $R(t/{}^3\text{He})$ measured by the FOPI collaboration [81] can not be reproduced with a single model [62]. More interestingly, the results of the INDRA experiment suggest that the triton and ${}^3\text{He}$ isobars seem to dominate the neutron enrichment of the neck zone [54]. However, the existence of “ ${}^3\text{He}$ -puzzle” in the coincidence events of LCPs and fission fragments is still an uncertain issue.

Due to the enriched but not-well-understood information carried by triton and ${}^3\text{He}$ coupling to both the isospin transport and the neck emission during fission process in HIRs, we are motivated to explore the emission of these two isobars in coincidence with fission fragments by inspecting the energy spectra and the yield ratio $R(t/{}^3\text{He})$ over wide angular range, and to bridge the ratio $R(t/{}^3\text{He})$ and the feature of fission process, as well as to infer the slope parameter of $E_{\text{sym}}(\rho)$. In this article, the energy spectra of triton and ${}^3\text{He}$ in coincidence with fission fragments at different angles are measured in the reactions of ${}^{86}\text{Kr} + {}^{\text{nat}}\text{Pb}$ at 25 MeV/u. The distributions of $R(t/{}^3\text{He})$ with respect to the fission plane and as a function of the laboratory polar angle are analyzed. The comparison of the experimental data to the transport model simulation is discussed. The paper is organized as following. Section II and III present the experimental setup and the description of the transport model, respectively. Section IV is the results and the discussions, and section V is the summary.

II. EXPERIMENTAL SETUP

The experiment was conducted at the Compact Spectrometer for Heavy Ion Experiment (CSHINE) [82, 83], built at the final focal plane of the Radioactive Ion Beam Line at Lanzhou (RIBLL-I) [84]. The ${}^{86}\text{Kr}$ beam of 25 MeV/u was extracted from the cyclotron of the Heavy Ion Research Facility at Lanzhou (HIRFL) [85], bombarding a natural lead target installed in the scattering chamber with the radius $R \approx 750$ mm. The target thickness is about 1 mg/cm². Fig. 1

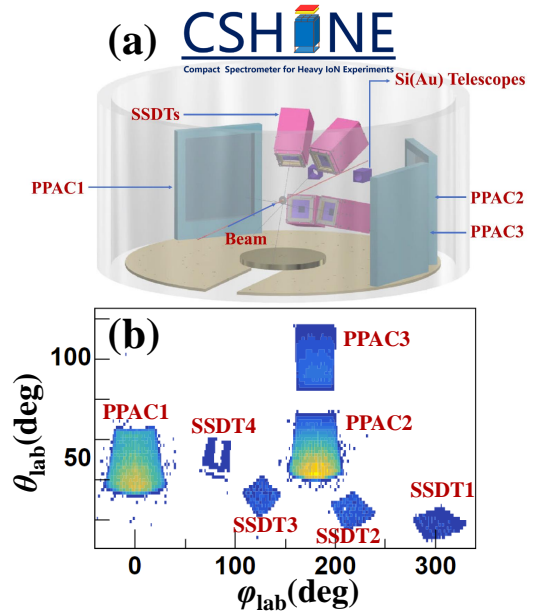


Fig. 1. (Color online) (a) The experimental setup of CSHINE. (b) The spatial coverage of SSDTs and PPACs on $\theta - \varphi$ plane in laboratory reference frame.

presents the experimental setup (a) and the spatial coverage of the silicon-strip detector telescopes (SSDTs) and the parallel plate avalanche counters (PPACs) (b).

The LCPs from the reactions were measured by 4 SSDTs, covering the angular range from 10° to 60° in laboratory. Each SSDT consists of three layers, namely, one single-sided silicon-strip detector (SSSSD) for ΔE_1 and one double-sided silicon strip detector (DSSSD) for ΔE_2 , backed by a 3×3 CsI(Tl) crystal hodoscope with the length of 50 mm for the energy deposit E . The granularity of the SSDT is $4 \times 4 \text{ mm}^2$, giving about 1° angular resolution. The energy resolution of the SSDT is better than 2%, and the isotopes up to $Z = 6$ can be identified [36]. Multi hits and signal sharing are carefully treated in the track recognition, and the track recognition efficiency is about 90% [86]. Fig. 2 shows the particle identification of light particles for this analysis. Panel (a) to (d) presents the scattering plot of $\Delta E_2 - E_{\text{CsI}}$ of the four SSDTs. The results show that $Z \leq 3$ LCPs, including triton and ${}^3\text{He}$, were identified clearly in each SSDT, supporting the reliability of the experimental results.

In order to explore the isospin properties of fission process, the fission fragments (FFs) were detected by 3 PPACs, each of which had a sensitive area of $240 \times 280 \text{ mm}^2$ [87, 88]. The perpendicular distance of the PPACs to the target is about 428 mm. The coverage of the PPACs ensures a high efficiency to measure the FFs in coincidence with the LCPs. And the trigger system is established to selected the fission events [89]. The working voltage of the PPACs can suppress the light charged particles significantly, although the specific values of mass and charge for FFs were not accurately determined. According to the previous source test results [82], the detection efficiency is almost 100% for FFs and negligibly low for light

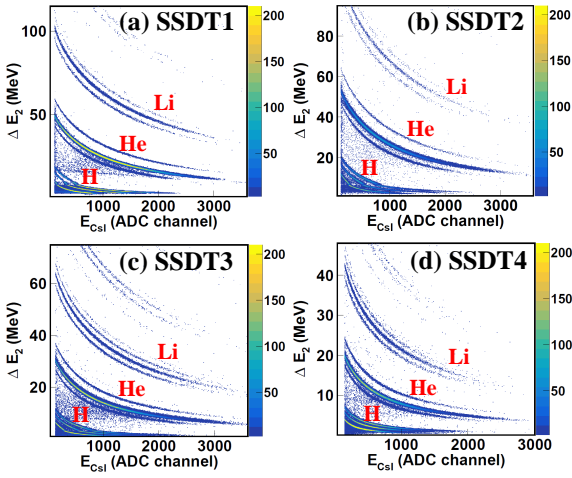


Fig. 2. (Color online) $\Delta E_2 - E_{\text{CSI}}$ plots of the four SSDTs.

163 particles with the detector condition ($\text{HV}=460$ V) as adopted
164 in the experiment. So, the PPACs can only be fired by heavy
165 fragments, rather than LCPs or IMFs.

166 Referring to the energy loss calculations only, the
167 projectile-like fragments (PLF) and target-like fragments
168 (TLF) may fire the PPACs as well. However, the geomet-
169 ric coverage of the PPACs in the experiment suppresses the
170 PLF and TLF. Otherwise because PLFs and TLFs are well
171 separated in velocity ($v_{\text{PLF}} \approx 6.8$ cm/ns, $v_{\text{TLF}} \approx 1.2$ cm/ns
172 at small linear momentum transfer or in peripheral reactions),
173 one shall be able to see two components clearly on the veloc-
174 ities of the two coincident fragments recorded in the PPACs.
175 Indeed, the two-component feature is not visible in the ve-
176 locity scattering plot (see Fig. 11 in [87]), it is safe and rea-
177 sonable to speculate that the heavy fragments detected with
178 PPACs in the experiment are mainly fission fragments.

III. THEORETICAL MODEL

180 A hybrid model by the improved quantum molecular dy-
181 namics model (ImQMD05) coupled with statistical decay af-
182 terburner (GEMINI) was used for theoretical simulation in
183 this work. The ImQMD05 [90] was used to simulate the nu-
184 cleon transport process in HIRs. And the GEMINI [91, 92]
185 was appended to obtain the final state productions of the reac-
186 tions. The ImQMD05 model is an improved version from the
187 original quantum molecular dynamics code [93, 94], and is
188 widely used to understand the dynamics of nuclear reactions
189 induced by heavy ions or light nuclei at both low and inter-
190 mediate energies [40, 41, 95–97]. The mean field part of the
191 ImQMD05 model used here includes the symmetry potential
192 energy part. And the local nuclear potential energy density
193 functional in the ImQMD05 model is written as

$$V_{\text{loc}} = \frac{\alpha}{2} \frac{\rho^2}{\rho_0} + \frac{\beta}{\eta+1} \frac{\rho^{\eta+1}}{\rho_0^\eta} + \frac{g_{\text{sur}}}{2\rho_0} (\nabla\rho)^2 \quad (1)$$

$$+ \frac{g_{\text{sur,iso}}}{\rho_0} [\nabla(\rho_n - \rho_p)]^2 + g_{\rho\tau} \frac{\rho^{8/3}}{\rho_0^{5/3}} + \frac{C_s}{2} \frac{\rho^{\gamma+1}}{\rho_0^\gamma} \delta^2,$$

194 where ρ , ρ_n and ρ_p are the density of nucleon, neutron and
195 proton, respectively. $\delta = (\rho_n - \rho_p)/(\rho_n + \rho_p)$ is the isospin
196 asymmetry degree. The parameters in Eq. (1) except C_s ,
197 which are listed in Table 1, are obtained directly from Skyrme
198 interaction with MSL0 parameter set [98]. C_s is determined
199 by the symmetry potential energy at saturation density. To-
200 gether with different values of γ , one can get the MSL0-like
201 Skyrme interaction with various density dependent symmetry
202 potential energy. After scanning the impact parameter up to
203 16.0 fm, the most probable weight of the fission events fil-
204 tered by experimental conditions is located at 7.0 fm. Hence,
205 the reaction was simulated with impact parameter in the range
206 of $1.0 \leq b \leq 7.0$ fm by a step of $\Delta b = 1.5$ fm. At the end
207 of the dynamical evolution in ImQMD05, setting at 500 fm/c,
208 the minimum spanning tree (MST) algorithm [94, 99] was
209 used to recognize the free nucleons and fragments formed in
210 the evolution. Next, the statistical decay of excited fragments
211 was performed with GEMINI afterburner. At last, the infor-
212 mation of final state particles will be obtained.

IV. RESULTS AND DISCUSSIONS

A. Characterizing the fission events

213 We start with the analysis of the orientation of the fis-
214 sion plane with respect to the beam direction. The fission
215 plane is reconstructed by the velocity of two FFs, using
216 $\vec{n}_{\text{FF}} = (\vec{v}_{F_1} \times \vec{v}_{F_2}) / |\vec{v}_{F_1}| |\vec{v}_{F_2}|$ to denote the normal vector of the
217 fission plane, as shown in Fig. 3 (a). Defining α_1 as the angle
218 between \vec{n}_{FF} and the beam direction \vec{v}_{beam} , one can charac-
219 terize how much the fission plane deviates from the beam.
220 The distribution of $|\cos(\alpha_1)|$ is peaked at 0 with a rather small
221 width $\sigma_{\alpha_1} \approx 6^\circ$, as shown in Fig. 3(b), inferring that the
222 fission plane keeps approximately the memory of the initial
223 angular momentum of the rotating system. With $Z \geq 10$ as
224 the condition to identify FFs for theoretical calculations, the
225 transport model prediction about the distribution of $|\cos(\alpha_1)|$
226 is in rather agreement with the experiment. The scattering
227 plots of folding angle vs. $|\cos(\alpha_1)|$ provide the information
228 of fission and detection geometry. With the detector filter of
229 PPACs on both θ_{lab} and ϕ_{lab} according to the setup, the ex-
230 perimental folding angle in Fig. 3(c) can be approximately
231 described by the model simulation in Fig. 3(d).

232 The characteristics of this rotating fissioning system was
233 obtained using the experiment data and theoretic simulations.
234 First, to estimate its charge and mass, the linear momentum
235 transfer (LMT) should be estimated experimentally. Assum-
236 ing a symmetric fission processes, the velocity of the fission-
237 ing system (FS) can be simply calculated by

TABLE 1. Parameter set used in the ImQMD05 calculations.

α (MeV)	β (MeV)	η (MeV fm ²)	g_{sur} (fm ²)	$g_{\text{sur,iso}}$ (fm ²)	$g_{\rho\pi}$ (MeV)	C_s (MeV)	ρ_0 (fm ⁻³)
-254	185	5/3	21.0	-0.82	5.51	36.0	0.160

$$\vec{v}_{\text{FS}} = \frac{1}{2}(\vec{v}_{\text{F1}} + \vec{v}_{\text{F2}}), \quad (2)$$

where \vec{v}_{F1} and \vec{v}_{F2} are the velocities of the two FFs, respectively. The LMT is defined as

$$\text{LMT} = \frac{A_{\text{tar}} \cdot v_{\text{FS}}^Z}{A_{\text{pro}} \cdot (v_{\text{pro}} - v_{\text{FS}}^Z)}, \quad (3)$$

Here the subscripts *pro* and *tar* denotes the projectile and target, respectively. v_{FS}^Z is the projection of \vec{v}_{FS} on the beam direction. As shown in Fig. 4, the distribution of the LMT derived from the experimental data is peaked in the vicinity of 0.4. The small peak below LMT < 0.2 is contributed by the fission events triggered by PPAC 1 and PPAC 3. Accordingly, the typical charge and mass of the rotating fission system are $Z_{\text{FS}} \approx Z_{\text{tar}} + Z_{\text{pro}} \cdot \text{LMT} = 96$ and $A_{\text{FS}} \approx A_{\text{tar}} + A_{\text{pro}} \cdot \text{LMT} = 242$.

Second, to estimate the angular momentum of the rotating fission system, one needs the most probable impact parameter, which can be determined by the event weight obtained from transport model simulations filtered by experimental conditions. Defining the fission event weight by

$$W_F = b \frac{n_F}{N_{\text{tot}}(b)}, \quad (4)$$

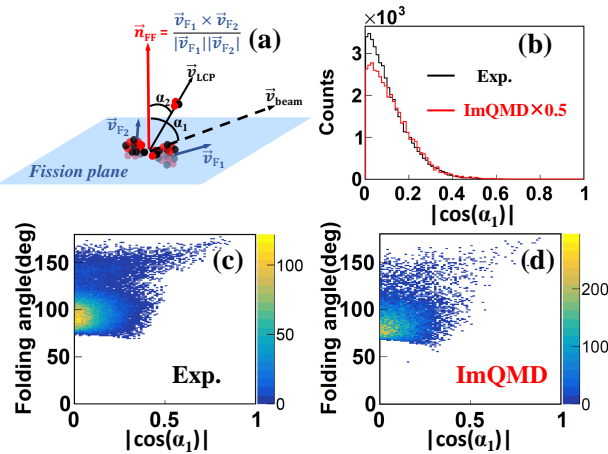


Fig. 3. (Color online) (a) Geometric diagram of fission plane of FFs and LCP emission. (b) Angular distribution between the normal vector \vec{n}_{FF} of the fission plane and the beam direction \vec{v}_{beam} . The experimental (c) and simulation (d) results of the folding angle *vs.* $|\cos(\alpha_1)|$ are shown in the bottom panels.

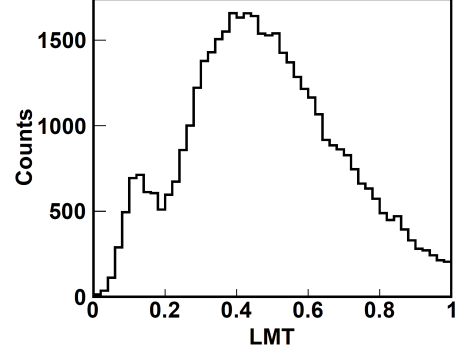


Fig. 4. (Color online) Experimental distribution of LMT.

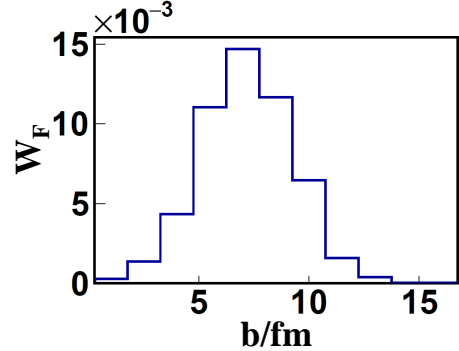


Fig. 5. (Color online) The weight of the fission events as a function of impact parameter b in ImQMD05 simulations.

where n_F is the number of fission events among N_{tot} events simulated at a given impact parameter b .

Fig. 5 shows the distribution of W_F , where the most probable impact parameter b_m is located in the vicinity of 7 fm.

The distance between the transferred part of the projectile and the mass center of the fissioning system is defined as

$$D = b_m \frac{A_{\text{tar}}}{A_{\text{tar}} + A_{\text{pro}} \cdot \text{LMT}}, \quad (5)$$

where $b_m = 7$ fm, $A_{\text{tar}} = 208$, $A_{\text{pro}} = 86$ and $\text{LMT} = 0.4$, respectively.

The angular momentum is written as

$$J = P_{\text{pro}} \cdot \text{LMT} \cdot D, \quad (6)$$

where $P_{\text{pro}} = 18700$ MeV/c and $D \approx 6$ fm was derived with $\text{LMT} = 0.4$. Then, the angular momentum of the rotating system is approximately $J \approx 200 \hbar$.

268 Third, to estimate the excitation energy of the rotating fission system, the moment of inertia I of a spherical nucleus 269 with the mass M_{FS} is 270

$$I = \frac{2}{5} M_{\text{FS}} r_{\text{FS}}^2, \quad (7)$$

271 where $r_{\text{FS}} = 1.4 A_{\text{FS}}^{1/3}$ fm is the radius of the fissioning system. 272 The rotating energy $E_{\text{rot}} = J^2/2I \approx 100$ MeV is approximately obtained. Ignoring the reaction Q value, the excitation 273 energy could be extracted by 274

$$E^* = E_{\text{kin}}^{\text{i}} - E_{\text{kin}}^{\text{f}} - E_{\text{rot}}, \quad (8)$$

275 where $E_{\text{kin}}^{\text{i}}$ and $E_{\text{kin}}^{\text{f}}$ are the initial state kinetic energy and 276 the final state kinetic energy, respectively. Approximately, 277 one has $E^* \approx 600$ MeV. The excitation energy is close to 278 the one of the fission system formed in 25 MeV/u Ar+Au at 279 LMT $\approx 80\%$, where the E^* was calculated by the pre-scission 280 α multiplicity [100]. For additional properties of fission systems, such as Viola systematics and angular distribution of 281 the fission axis, please refer to our previously published paper 282 per [87].

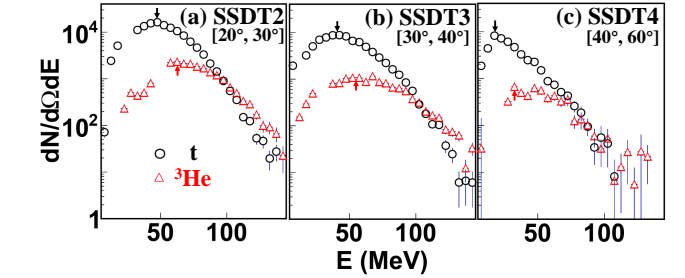


Fig. 6. (Color online) The experimental energy spectra of triton (circle) and ${}^3\text{He}$ (triangle) in $20^\circ \leq \theta_{\text{lab}} \leq 60^\circ$ covered by SSDT2 to SSDT4 in coincidence with two FFs. The arrows represent the peak position of each experimental energy spectrum.

305 the Coulomb barrier higher than that of triton [74]. In coalescence scenario, which was applied to interpret the difference 306 between ${}^3\text{He}$ and α particles [78], the former is dominantly produced by the coalescence of preequilibrium nucleons, delivering larger mean kinetic energy. These two explanations 307 are qualitatively in agreement, supporting that ${}^3\text{He}$ is 308 predominantly emitted at earlier stage. Our experimental results 309 show that the “ ${}^3\text{He}$ -puzzle” exists in the events tagged 310 by fission. It suggests that the puzzle exists in both inclusive 311 and fission events.

284 B. Analysis of the energy spectra of t and ${}^3\text{He}$

285 We now present the analysis of the emission of triton and 286 ${}^3\text{He}$ in the (fast)fission events. The energy spectra of LCPs in 287 coincidence with FFs contain thermal and dynamical information 288 of the particles emitted from the fission events. Fig. 289 6 presents the energy spectra of triton (open circles) and ${}^3\text{He}$ 290 (open triangles) emitted from fission events in different angular ranges corresponding to SSDTs 2 to 4. To reduce the 291 contamination of quasi-projectiles, the data of SSDT1 covering 292 $10^\circ - 20^\circ$ in the laboratory is not counted here. It is shown 293 that the spectrum of ${}^3\text{He}$ is generally harder than that of triton, 294 leading to a larger average kinetic energy of the former. The 295 difference between triton and ${}^3\text{He}$ is more pronounced at 296 forward angles than at large angles. This observation of “ ${}^3\text{He}$ -puzzle” 297 is in accordance with the previous inclusive measurements 298 at high beam energies [73, 75–77, 81, 101–104].

TABLE 2. Energy peak position E_p of triton and ${}^3\text{He}$ for SSDT 2 to 4.

	SSDT2	SSDT3	SSDT4
E_p of triton (MeV)	45	40	19
E_p of ${}^3\text{He}$ (MeV)	62	58	38

300 The “ ${}^3\text{He}$ -puzzle” has been interpreted by two possible scenarios: sequential decay [74] and coalescence model [78]. In 301 the sequential decay scenario, the difference between ${}^3\text{He}$ and 302 triton is influenced by the Coulomb barrier, for which ${}^3\text{He}$ is 303 emitted at an earlier stage with high temperature to overcome 304

315 C. Out-of-plane emission and the effect of $E_{\text{sym}}(\rho)$

316 Benefiting from the wide angular coverage of the SSDTs 317 and PPACs in laboratory reference frame, the angular behavior 318 of the particle emission can be analyzed. To compare the 319 yields of particles with different energy spectrum behaviors 320 and avoid the influence of the possible experimental distortion 321 caused by the energy threshold in each SSDTs, a data 322 adaptive energy spectrum peak cut scenario is applying. We 323 focus on the descending part on the high energy side of the 324 energy peak. The energy peak positions (E_p) are listed in Table 325 2. Meanwhile, using the energy condition $E \geq E_p$ as the low 326 limit cut, one can suppress the interference of the evaporation 327 process and emphasize the feature of the dynamic emission.

328 The angular distribution of $R(t/{}^3\text{He})$ as a function of the 329 polar angle in laboratory θ_{lab} is generated with events of 330 one LCP in coincidence with two FFs, as shown in Fig. 331 7. The same energy threshold, geometry and folding angle 332 cuts are applied to both experimental and simulation results. 333 It is shown that for the wide angular range, the distribution 334 exhibits a rising trend. This feature is consistent 335 with the moving source picture, where the neutron richness 336 of particle emission increases from the projectile-like 337 source to the medium velocity source corresponding to the 338 neck, as predicted by various transport model simulations 339 [40, 41, 46, 48, 49, 51, 105–109], and experimentally ob- 340 served in a specific angular window [42, 45, 50, 54, 79, 110– 341 112] or a parallel velocity window [45, 79, 80, 113–118].

342 In order to see the symmetry energy effect, a soft ($\gamma = 0.5$) 343 and a stiff ($\gamma = 1.0$) symmetry energy are adopted in

the ImQMD05 simulations. These two γ values correspond to slope parameter of $E_{\text{sym}}(\rho)$ with $L = 51$ and 77 MeV at ρ_0 , respectively. Although the predicted value of $R(t/{}^3\text{He})$ is far off to the experiment, the rising trend of $R(t/{}^3\text{He})$ as a function of θ_{lab} was reproduced by model simulations in both γ cases. In order to quantify the increasing rate, the function of $f(x) = e^{(p_0+p_1x)}$ is applied to fit the data and the model predictions, respectively. The parameter p_1 describes the increasing rate of $R(t/{}^3\text{He})$ to θ_{lab} . As shown in Fig. 7, the rising trend depends on γ . Visibly, a softer $E_{\text{sym}}(\rho)$ causes a relative larger increasing rate. When comparing the fitting results between experiment and model in Table 3, the value of experimental p_1 is marginally located between $\gamma = 0.5$ and 1.0 . Nevertheless, the large uncertainty here reduces the sensitivity and hinder to make a convincing constraint of $E_{\text{sym}}(\rho)$.

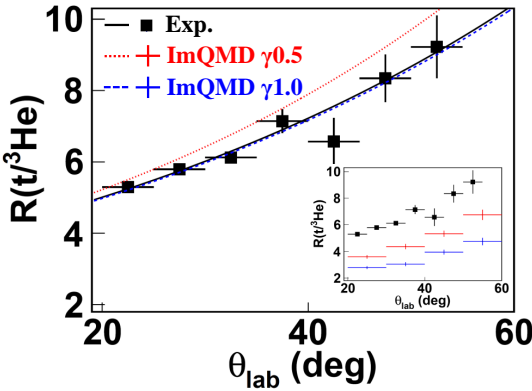


Fig. 7. (Color online) The ratio $R(t/{}^3\text{He})$ as a function of θ_{lab} . The black solid squares and black line represent the experiment data and fitting result with $E \geq E_p$ cuts in coincidence with fission events. The red and blue cross markers represent the ImQMD05 calculations data of $\gamma = 0.5$ and 1.0 in the inset. The red dot and blue dash lines are the fitting results of $\gamma = 0.5$ and 1.0 which is normalized with experimental fitting result of p_0 .

TABLE 3. Fitting results of the ratio $R(t/{}^3\text{He})$ as a function of θ_{lab} using $f(x) = e^{(p_0+p_1x)}$

	p_0	p_1
Experiment	1.25 ± 0.06	0.018 ± 0.002
$\gamma=0.5$	0.75 ± 0.08	0.021 ± 0.002
$\gamma=1.0$	0.54 ± 0.09	0.018 ± 0.002

It is then motivated to go a further step to find a novel probe, of which the fission event topology is better controlled and the sensitivity on $E_{\text{sym}}(\rho)$ can be enhanced. Fig. 8 presents the angular distribution of $R(t/{}^3\text{He})$ with respect to the fission plane. The α_2 on the abscissa is the relative angle between \vec{n}_{FF} and the velocity of the coincident triton or ${}^3\text{He}$ \vec{v}_{LCP} as shown in Fig. 3 (a), with $|\cos(\alpha_2)| = 0$ (1) corresponding to in-plane (out-of-plane) emission. Again, the same cuts are applied for both experimental and theoretical results. The increasing trend of $R(t/{}^3\text{He})$ with $|\cos(\alpha_2)|$ indicates that the neutron rich particles emitted from out-of-fission-plane is enhanced. This phenomenon is the consequence of the competi-

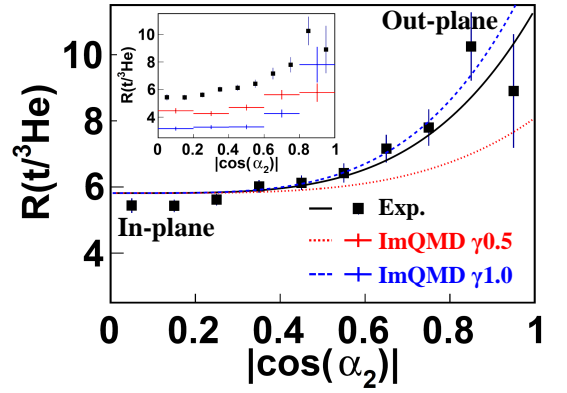


Fig. 8. (Color online) The ratio $R(t/{}^3\text{He})$ as a function of $|\cos(\alpha_2)|$. The black solid squares and black line represent the experiment data and fitting result. The red and blue cross markers represent the theoretical calculations data of $\gamma = 0.5$ and 1.0 in the inset. The red dot and blue dash lines are the fitting results of $\gamma = 0.5$ and 1.0 which is normalized with experimental fitting result of p_0

TABLE 4. Fitting results of $R(t/{}^3\text{He})$ as a function of $|\cos(\alpha_2)|$ using $f(x) = p_0 + p_1x^4$.

	p_0	p_1
Experiment	5.8 ± 0.2	5.5 ± 1.6
$\gamma=0.5$	4.5 ± 0.1	2.3 ± 1.1
$\gamma=1.0$	3.0 ± 0.1	6.8 ± 1.8

tion between the isospin migration and the centrifugal motion of the particles in the rotating fission system. When the reaction system is viewed as a rotating emission source, particles emitted near the fission plane are subjected to stronger centrifugal potential during the emission process, weakening the difference between neutrons and protons under the isovector potential. From the in-plane to out-of-plane, more neutron rich particles are emitted due to the effect of isospin fractionation [67], indicating that the effect of the isovector potential becomes more significant compared to centrifugal potential. This observation gives us the chance to explore the properties of isospin transport and the density dependence of $E_{\text{sym}}(\rho)$ in (fast)fission reactions.

Similarly, to describe the increasing trend of the angular distribution of $|\cos(\alpha_2)|$, the function of $f(x) = p_0 + p_1x^4$ is used to fit data and the simulations. Again, p_0 is far off to the experiment due to the clustering difficulty of transport model, but the parameter p_1 can be used to describe the increasing rate of the ratio with out-of-plane angle. In Fig. 8, the fitting curves exhibit a different increasing behavior between $\gamma = 0.5$ and 1.0 , indicating that the enhancement of neutron rich particle emission out of fission plane is sensitive to the form of $E_{\text{sym}}(\rho)$. Inspecting the increasing curves and the values of p_1 as listed in Table 4, one finds that the experimental increasing rate situates between the theoretical prediction with $\gamma = 0.5$ and 1.0 , in accordance with the conclusion of our previous work [36], where a totally different probe was used. The

398 comparison seems to exclude very soft ($\gamma < 0.5$) and very stiff
 399 ($\gamma > 1.0$) candidates of symmetry energy. The results indicate that the ratio $R(t/{}^3\text{He})$ as a function of $|\cos(\alpha_2)|$ seems
 400 to be a sensitive probe for density dependent symmetry energy, especially in the larger $|\cos(\alpha_2)|$ range, which is very
 401 close to the boundary of the current detector coverage. Hence,
 402 more events in the larger $|\cos(\alpha_2)|$ range are preferentially re-
 403 quested in the further experiments. Data analysis of a new
 404 measurement of ${}^{86}\text{Kr} + {}^{124}\text{Sn}$ at 25 MeV/u is ongoing [119].

407 Fig. 9 shows in addition the relationship between $|\cos(\alpha_2)|$
 408 and θ_{lab} with the experiment events of triton in coincidence
 409 with two fission fragments. Visibly, there is a weak positive
 410 correlation between $|\cos(\alpha_2)|$ and θ_{lab} . The origin of the cor-
 411 relation is partly due to the fact that the azimuth coverage of
 412 the PPAC is quite limited. With such weak correlation, one in-
 413 fers that the two distributions shown in Fig. 7 and Fig. 8 have
 414 their own implications. Namely, the distribution of $R(t/{}^3\text{He})$
 415 as a function of θ_{lab} indicates that the low density and neu-
 416 tron rich medium velocity emission source (neck) is formed,
 417 while the distribution of $R(t/{}^3\text{He})$ as a function of $|\cos(\alpha_2)|$
 418 characterizes the fine out-of-plane properties of the isospin
 419 transport in a fissioning process. Upon comparing the results
 420 presented in Table 3 and Table 4, it becomes evident that the
 421 enhancement of $R(t/{}^3\text{He})$ vs. $|\cos(\alpha_2)|$, particularly at larger
 422 out-of-plane angles, appears to be a more sensitive probe for
 423 studying nuclear symmetry energy than the polar angular dis-
 424 tribution of $R(t/{}^3\text{He})$. In another word, in the properly charac-
 425 terized fission events, the effect of $E_{\text{sym}}(\rho)$ can be magnified,
 426 supporting the previous predictions by transport model simu-
 427 lations [40].

428 Currently we do not attempt to make a fine tuning and con-
 429 straint of γ parameter in the simulations, since the absolute
 430 value of $R(t/{}^3\text{He})$ is not yet well reproduced, as indicated by
 431 Fig. 7 and 8. Further studies are required in transport model
 432 in order to elucidate the origin and the formation mechanism
 433 of light clusters including triton and ${}^3\text{He}$. Recently, the yield
 434 of light clusters is better reproduced by introducing Mott ef-
 435 fect in transport model [120]. Meanwhile, the cooling pro-

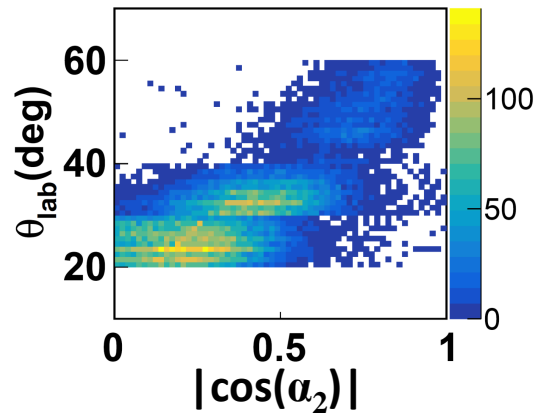


Fig. 9. (Color online) The scattering plot between $|\cos(\alpha_2)|$ and laboratory angle with the experiment events of triton in coincidence with two fission fragments.

436 cess of the rotating fissioning system with similar E^* and J
 437 is of high interest. We are going to make further calculations
 438 on particle emission from a rotating system with inclusion of
 439 deuteron, triton and ${}^3\text{He}$ apart of neutron, proton and α par-
 440 ticles, as done in [121]. The emission of other particles than
 441 $A=3$ isobars may bring significant effect to the featured dis-
 442 tribution of the latter in the cooling process of the fissioning
 443 system.

V. SUMMARY

444 The energy spectra and angular distributions of triton and
 445 ${}^3\text{He}$ ranging from 20° to 60° in the laboratory in coinci-
 446 dence with fission fragments are analyzed in 25 MeV/u ${}^{86}\text{Kr} + {}^{\text{nat}}\text{Pb}$
 447 reactions. It is shown that the energy spectra of ${}^3\text{He}$ are gen-
 448 erally harder than triton even in the fission events, and the
 449 effect is more pronounced at small angles. Applying a data
 450 driven energy spectrum peak cut scenario, the rising trend
 451 of angular distribution of $R(t/{}^3\text{He})$ is observed in the coinci-
 452 dent events of one LCP and two FFs, which is consistent with
 453 previous inclusive observations. The yield ratio $R(t/{}^3\text{He})$ ex-
 454 hibits an enhancement as a function of $|\cos(\alpha_2)|$, evidencing
 455 more neutron rich particles emitted from out-of-fission-plane.
 456 With a qualitative comparison with ImQMD05 simulations,
 457 the enhancement of neutron rich particle emission from out-
 458 of-fission-plane seems to be a novel probe for nuclear symme-
 459 try energy. More measurements at large out-of-fission-plane
 460 angles and further theoretic investigations are required for a
 461 stringent constraint of $E_{\text{sym}}(\rho)$.

VI. ACKNOWLEDGEMENT

463 This work is supported by the National Natural Sci-
 464 ence Foundation of China under Grant Nos. 12205160,
 465 11961131010, 11961141004, and 11965004, and by the
 466 Ministry of Science and Technology of China under Nos.
 467 2022YFE0103400 and 2020YFE0202001, and by the Polish
 468 National Science Center under No. 2023/49/B/ST2/01294.
 469 This work is also supported by Initiative Scientific Research
 470 Program and the Center of High Performance Computing of
 471 Tsinghua University, and the Heavy Ion Research Facility at
 472 Lanzhou (HIRFL). The authors thank Huigan Cheng from
 473 SCUT, Zhen Zhang from SYSU and Rui Wang from INFN
 474 for their valuable discussions.

- [1] B. A. Li, B. J. Cai, W. J. Xie et al., Progress in Constraining Nuclear Symmetry Energy Using Neutron Star Observables Since GW170817. *Universe*, **7**(6):182, (2021). doi: [10.3390/universe7060182](https://doi.org/10.3390/universe7060182)
- [2] S. Huth, P. T. H. Pang, I. Tews et al., Constraining Neutron-Star Matter with Microscopic and Macroscopic Collisions, *Nature* **606**, 276-280 (2022). doi: [10.1038/s41586-022-04750-w](https://doi.org/10.1038/s41586-022-04750-w)
- [3] A. W. Steiner, M. Prakash, J. M. Lattimer et al., Isospin asymmetry in nuclei and neutron stars, *Phys. Rept.* **411**, 325-375 (2005). doi: [10.1016/j.physrep.2005.02.004](https://doi.org/10.1016/j.physrep.2005.02.004)
- [4] M. Oertel, M. Hempel, T. Klähn et al., Equations of state for supernovae and compact stars, *Rev. Mod. Phys.* **89**, 015007 (2017). doi: [10.1103/RevModPhys.89.015007](https://doi.org/10.1103/RevModPhys.89.015007)
- [5] B. A. Li, A. Ramos, G. Verde et al., Topical issue on nuclear symmetry energy, *Eur. Phys. J. A* **50**, 9 (2014). doi: [10.1140/epja/i2014-14009-x](https://doi.org/10.1140/epja/i2014-14009-x)
- [6] B. A. Li, L. W. Chen and C. M. Ko, Recent Progress and New Challenges in Isospin Physics with Heavy-Ion Reactions, *Phys. Rept.* **464**, 113-281 (2008). doi: [10.1016/j.physrep.2008.04.005](https://doi.org/10.1016/j.physrep.2008.04.005)
- [7] B. P. Abbott et al. [LIGO Scientific and Virgo], GW170817: Observation of Gravitational Waves from a Binary Neutron Star Inspiral, *Phys. Rev. Lett.* **119**, 161101 (2017). doi: [10.1103/PhysRevLett.119.161101](https://doi.org/10.1103/PhysRevLett.119.161101)
- [8] B. P. Abbott et al. [LIGO Scientific and Virgo], GW170817: Measurements of neutron star radii and equation of state, *Phys. Rev. Lett.* **121**, 161101 (2018). doi: [10.1103/PhysRevLett.121.161101](https://doi.org/10.1103/PhysRevLett.121.161101)
- [9] S. De, D. Finstad, J. M. Lattimer, D. A. Brown et al., Tidal Deformabilities and Radii of Neutron Stars from the Observation of GW170817, *Phys. Rev. Lett.* **121**, 091102 (2018). doi: [10.1103/PhysRevLett.121.091102](https://doi.org/10.1103/PhysRevLett.121.091102)
- [10] M. Q. Ding, D. Q. Fang and Y. G. Ma, Neutron skin and its effects in heavy-ion collisions, *Nucl. Sci. Tech.* **35**, no.12, 211 (2024) . doi: [10.1007/s41365-024-01584-1](https://doi.org/10.1007/s41365-024-01584-1)
- [11] T. Z. Yan, S. Li, Isotopic dependence of the yield ratios of light fragments from different projectiles and their unified neutron skin thicknesses, *Nucl. Sci. Tech.* **35**, no.65 (2024) . doi: [10.1007/s41365-024-01425-1](https://doi.org/10.1007/s41365-024-01425-1)
- [12] W. J. Xie, Z. W. Ma and J. H. Guo, Bayesian inference of the crust-core transition density via the neutron-star radius and neutron-skin thickness data, *Nucl. Sci. Tech.* **34**, no.91 (2023) . doi: [10.1007/s41365-023-01239-7](https://doi.org/10.1007/s41365-023-01239-7)
- [13] D. Q. Fang, "Neutron skin thickness and its effects in nuclear reactions." *Nucl. Tech.* **46**, 080016, (2023). doi: [10.11889/j.0253-3219.2023.hjs.46.080016](https://doi.org/10.11889/j.0253-3219.2023.hjs.46.080016)
- [14] R. An, S. Sun, L. G. Cao, et al., New quantification of symmetry energy from neutron skin thicknesses of ^{48}Ca and ^{208}Pb , *Nucl. Sci. Tech.* **35**, no.10, 182 (2024) . doi: [10.1007/s41365-024-01551-w](https://doi.org/10.1007/s41365-024-01551-w)
- [15] R. An, S. Sun, L. G. Cao, et al., Constraining nuclear symmetry energy with the charge radii of mirror-pair nuclei, *Nucl. Sci. Tech.* **34**, no.8, 119 (2023) . doi: [10.1007/s41365-023-01269-1](https://doi.org/10.1007/s41365-023-01269-1)
- [16] F. P. Li, L. G. Pang, X. N. Wang, Application of machine learning to the study of QCD transition in heavy ion collisions, *Nucl. Tech.* **46**, 040014, (2023). doi: [10.11889/j.0253-3219.2023.hjs.46.040014](https://doi.org/10.11889/j.0253-3219.2023.hjs.46.040014)
- [17] Y. Y. Liu, J. P. Yang, Y. J. Wang, et al., A perspective on describing nucleonic flow and pionic observables within the ultra-relativistic quantum molecular dynamics model, *Nucl. Sci. Tech.* **36**, no.3, 45 (2025). doi: [10.1007/s41365-024-01607-x](https://doi.org/10.1007/s41365-024-01607-x)
- [18] S. N. Wei and Z. Q. Feng, Properties of collective flow and pion production in intermediate-energy heavy-ion collisions with a relativistic quantum molecular dynamics model, *Nucl. Sci. Tech.* **35**, no.1, 15 (2024). doi:[10.1007/s41365-024-01380-x](https://doi.org/10.1007/s41365-024-01380-x)
- [19] B. A. Li, C. M. Ko and Z. z. Ren, Equation of state of asymmetric nuclear matter and collisions of neutron rich nuclei, *Phys. Rev. Lett.* **78**, 1644 (1997). doi: [10.1103/PhysRevLett.78.1644](https://doi.org/10.1103/PhysRevLett.78.1644)
- [20] Y. X. Zhang and Z. X. Li, Probing the density dependence of the symmetry potential with peripheral heavy-ion collisions, *Phys. Rev. C* **71**, 024604 (2005). doi: [10.1103/PhysRevC.71.024604](https://doi.org/10.1103/PhysRevC.71.024604)
- [21] L. W. Chen, C. M. Ko and B. A. Li, Light clusters production as a probe to the nuclear symmetry energy, *Phys. Rev. C* **68**, 017601 (2003). doi: [10.1103/PhysRevC.68.017601](https://doi.org/10.1103/PhysRevC.68.017601)
- [22] B. A. Li, Probing the high density behavior of nuclear symmetry energy with high-energy heavy ion collisions, *Phys. Rev. Lett.* **88**, 192701 (2002). doi: [10.1103/PhysRevLett.88.192701](https://doi.org/10.1103/PhysRevLett.88.192701)
- [23] Z. Xiao, B. A. Li, L. W. Chen et al., Circumstantial Evidence for a Soft Nuclear Symmetry Energy at Suprasaturation Densities, *Phys. Rev. Lett.* **102**, 062502 (2009). doi: [10.1103/PhysRevLett.102.062502](https://doi.org/10.1103/PhysRevLett.102.062502)
- [24] J. Estee et al. [SpiRiT], Probing the Symmetry Energy with the Spectral Pion Ratio, *Phys. Rev. Lett.* **126**, 162701 (2021). doi: [10.1103/PhysRevLett.126.162701](https://doi.org/10.1103/PhysRevLett.126.162701)
- [25] Q. Li, Z. Li, S. Soff et al., Probing the density dependence of the symmetry potential at low and high densities, *Phys. Rev. C* **72**, 034613 (2005). doi: [10.1103/PhysRevC.72.034613](https://doi.org/10.1103/PhysRevC.72.034613)
- [26] G. Ferini, T. Gaitanos, M. Colonna et al., Isospin effects on sub-threshold kaon production at intermediate energies, *Phys. Rev. Lett.* **97**, 202301 (2006). doi: [10.1103/PhysRevLett.97.202301](https://doi.org/10.1103/PhysRevLett.97.202301)
- [27] G. C. Yong, B. A. Li, Z. G. Xiao et al., Probing the high-density nuclear symmetry energy with the $\Xi-\bar{\Xi}$ ratio in heavy-ion collisions at $s_{\text{NN}} \approx 3$ GeV, *Phys. Rev. C* **106**, 024902 (2022). doi: [10.1103/PhysRevC.106.024902](https://doi.org/10.1103/PhysRevC.106.024902)
- [28] J. Xu, Transport approaches for the description of intermediate-energy heavy-ion collisions, *Prog. Part. Nucl. Phys.* **106**, 312-359 (2019). doi: [10.1016/j.ppnp.2019.02.009](https://doi.org/10.1016/j.ppnp.2019.02.009)
- [29] Y. J. Wang and Q. F. Li, Application of microscopic transport model in the study of nuclear equation of state from heavy ion collisions at intermediate energies, *Front. Phys. (Beijing)* **15**, 44302 (2020). doi: [10.1007/s11467-020-0964-6](https://doi.org/10.1007/s11467-020-0964-6)
- [30] Y. X. Zhang et al., [TMEP], Comparison of heavy-ion transport simulations: Collision integral in a box, *Phys. Rev. C* **97**, 034625 (2018). doi: [10.1103/PhysRevC.97.034625](https://doi.org/10.1103/PhysRevC.97.034625)
- [31] A. Ono et al., [TMEP], Comparison of heavy-ion transport simulations: Collision integral with pions and Δ resonances in a box, *Phys. Rev. C* **100**, 044617 (2019). doi: [10.1103/PhysRevC.100.044617](https://doi.org/10.1103/PhysRevC.100.044617)
- [32] M. Colonna et al., [TMEP], Comparison of heavy-ion transport simulations: Mean-field dynamics in box, *Phys. Rev. C* **104**, 024603 (2021). doi: [10.1103/PhysRevC.104.024603](https://doi.org/10.1103/PhysRevC.104.024603)
- [33] Y. Zhang, J. Tian, W. Cheng et al., Long-time drift of the isospin degree of freedom in heavy ion collisions, *Phys. Rev. C* **95**, 041602 (2017). doi: [10.1103/PhysRevC.95.041602](https://doi.org/10.1103/PhysRevC.95.041602)

- [34] L. Ou, Z. Xiao, H. Yi et al., Dynamic Isovector Reorientation of Deuteron as a Probe to Nuclear Symmetry Energy, Phys. Rev. Lett. **115**, 212501 (2015). doi: [10.1103/PhysRevLett.115.212501](https://doi.org/10.1103/PhysRevLett.115.212501)
- [35] Y. Wang, F. Guan, Q. Wu, et al., The emission order of hydrogen isotopes via correlation functions in 30 MeV/u Ar+Au reactions, Phys. Lett. B **825**, 136856 (2022). doi: [10.1016/j.physletb.2021.136856](https://doi.org/10.1016/j.physletb.2021.136856)
- [36] Y. Wang, F. Guan, X. Diao et al., Observing the ping-pong modality of the isospin degree of freedom in cluster emission from heavy-ion reactions, Phys. Rev. C **107**, L041601 (2023). doi: [10.1103/PhysRevC.107.L041601](https://doi.org/10.1103/PhysRevC.107.L041601)
- [37] Y. Wang and Z. Xiao, Correlation function studies at intermediate energies at CSHINE, NUOVO CIMENTO C - COLLOQUIA AND COMMUNICATIONS IN PHYSICS **48**(1), JAN-FEB (2025). doi: [10.1393/ncc/i2025-25037-x](https://doi.org/10.1393/ncc/i2025-25037-x)
- [38] G. Poggi, Neck emissions and the isospin degree of freedom, Nucl. Phys. A **685**, 296-311 (2001). doi: [10.1016/S0375-9474\(01\)00548-6](https://doi.org/10.1016/S0375-9474(01)00548-6)
- [39] M. D. Toro, A. Olmi, R. Roy, Neck dynamics, Eur. Phys. J. A **30**, 65–70 (2006).. doi: [10.1140/epja/i2006-10106-9](https://doi.org/10.1140/epja/i2006-10106-9)
- [40] Q. Wu, F. Guan, X. Diao et al., Symmetry energy effect on emissions of light particles in coincidence with fast fission, Phys. Lett. B **811**, 135865 (2020). doi: [10.1016/j.physletb.2020.135865](https://doi.org/10.1016/j.physletb.2020.135865)
- [41] Q. Wu, X. Diao, F. Guan et al., Transport model studies on the fast fission of the target-like fragments in heavy ion collisions, Phys. Lett. B **797**, 134808 (2019). doi: [10.1016/j.physletb.2019.134808](https://doi.org/10.1016/j.physletb.2019.134808)
- [42] J. Toke, B. Lott, S. P. Baldwin et al., Intermediate-Mass Fragment Decay of the Neck Zone Formed in Peripheral $^{209}\text{Bi} + ^{136}\text{Xe}$ Collisions at $E_{\text{lab}}/\text{A}=28$ MeV, Phys. Rev. Lett. **75**, 2920–2923 (1995). doi: [10.1103/PhysRevLett.75.2920](https://doi.org/10.1103/PhysRevLett.75.2920)
- [43] J. F. Dempsey, R. J. Charity, L. G. Sobotka et al., Isospin dependence of intermediate mass fragment production in heavy-ion collisions at E/A=55 MeV, Phys. Rev. C **54**, 1710-1719 (1996). doi: [10.1103/PhysRevC.54.1710](https://doi.org/10.1103/PhysRevC.54.1710)
- [44] E. Ramakrishnan, H. Johnston, F. Gimeno-Nogues et al., Fragment emission from the mass-symmetric reactions $^{58}\text{Fe} + ^{58}\text{Ni}$, $^{58}\text{Fe} + ^{58}\text{Ni}$ at $E_{\text{beam}} = 30$ MeV/nucleon, Phys. Rev. C **57**, 1803-1811 (1998). doi: [10.1103/PhysRevC.57.1803](https://doi.org/10.1103/PhysRevC.57.1803)
- [45] S. Hudan, R. Alfaro, B. Davin et al., Comparison of mid-velocity fragment formation with projectile-like decay, Phys. Rev. C **71**, 054604 (2005). doi: [10.1103/PhysRevC.71.054604](https://doi.org/10.1103/PhysRevC.71.054604)
- [46] L. G. Sobotka, J. F. Dempsey, R. J. Charity et al., Clustered and neutron-rich low density 'neck' region produced in heavy-ion collisions, Phys. Rev. C **55**, 2109-2111 (1997). doi: [10.1103/PhysRevC.55.2109](https://doi.org/10.1103/PhysRevC.55.2109)
- [47] R. Laforest, E. Ramakrishnan, D. J. Rowland et al., Dependence of projectile fragmentation on target N/Z, Phys. Rev. C **59**, 2567-2573 (1999). doi: [10.1103/PhysRevC.59.2567](https://doi.org/10.1103/PhysRevC.59.2567)
- [48] Y. Zhang, C. Zhou, J. Chen et al., Correlation between the fragmentation modes and light charged particles emission in heavy ion collisions, Sci. China Phys. Mech. Astron. **58**, 112002 (2015). doi: [10.1007/s11433-015-5723-2](https://doi.org/10.1007/s11433-015-5723-2)
- [49] Z. Q. Feng, Effects of isospin dynamics on neck fragmentation in isotopic nuclear reactions, Phys. Rev. C **94**, 014609 (2016). doi: [10.1103/PhysRevC.94.014609](https://doi.org/10.1103/PhysRevC.94.014609)
- [50] A. Rodriguez Manso, A. B. McIntosh, A. Jedelev et al., Detailed characterization of neutron-proton equilibration in dynamically deformed nuclear systems, Phys. Rev. C **95**, 044604 (2017). doi: [10.1103/PhysRevC.95.044604](https://doi.org/10.1103/PhysRevC.95.044604)
- [51] H. S. Wang, J. Xu, B. A. Li et al., Reexamining the isospin-relaxation time in intermediate-energy heavy-ion collisions, Phys. Rev. C **98**, 054608 (2018). doi: [10.1103/PhysRevC.98.054608](https://doi.org/10.1103/PhysRevC.98.054608)
- [52] R. Bougault, E. Bonnet, B. Borderie et al., Light charged clusters emitted in 32 MeV/nucleon $^{136,124}\text{Xe} + ^{124,112}\text{Sn}$ reactions: Chemical equilibrium and production of ^3He and ^6He , Phys. Rev. C **97**, 024612 (2018). doi: [10.1103/PhysRevC.97.024612](https://doi.org/10.1103/PhysRevC.97.024612)
- [53] L. W. May, A. Wakhle, A. B. McIntosh et al., Neutron-proton equilibration in 35 MeV/u collisions of $^{64,70}\text{Zn} + ^{64,70}\text{Zn}$ and $^{64}\text{Zn}, ^{64}\text{Ni} + ^{64}\text{Zn}, ^{64}\text{Ni}$ quantified using triplicate probes, Phys. Rev. C **98**, 044602 (2018). doi: [10.1103/PhysRevC.98.044602](https://doi.org/10.1103/PhysRevC.98.044602)
- [54] Q. Fable et al., [INDRA], Experimental study of isospin transport with $^{40,48}\text{Ca} + ^{40,48}\text{Ca}$ reactions at 35 MeV/nucleon, Phys. Rev. C **107**, 014604 (2023). doi: [10.1103/PhysRevC.107.014604](https://doi.org/10.1103/PhysRevC.107.014604)
- [55] E. De Filippo and A. Pagano, Experimental effects on dynamics and thermodynamics in nuclear reactions on the symmetry energy as seen by the CHIMERA 4π detector, Eur. Phys. J. A **50**, 32 (2014). doi: [10.1140/epja/i2014-14032-y](https://doi.org/10.1140/epja/i2014-14032-y)
- [56] V. Baran, M. Colonna, M. Di Toro et al., Isospin effects in nuclear fragmentation, Nucl. Phys. A **703**, 603-632 (2002). doi: [10.1016/S0375-9474\(01\)01671-2](https://doi.org/10.1016/S0375-9474(01)01671-2)
- [57] V. Baran, M. Colonna and M. Di Toro, Neck fragmentation reaction mechanism, Nucl. Phys. A **730**, 329-354 (2004). doi: [10.1016/j.nuclphysa.2003.10.022](https://doi.org/10.1016/j.nuclphysa.2003.10.022)
- [58] V. Baran, M. Colonna, M. Di Toro et al., Isospin transport at Fermi energies, Phys. Rev. C **72**, 064620 (2005). doi: [10.1103/PhysRevC.72.064620](https://doi.org/10.1103/PhysRevC.72.064620)
- [59] M. Colonna, V. Baran and M. Di Tor, Theoretical predictions of experimental observables sensitive to the symmetry energy Eur. Phys. J. A **50**, 30 (2014). doi: [10.1140/epja/i2014-14030-1](https://doi.org/10.1140/epja/i2014-14030-1)
- [60] M. Colonna, Collision dynamics at medium and relativistic energies, Prog. Part. Nucl. Phys., 113:103775, (2020). doi: [10.1016/j.ppnp.2020.103775](https://doi.org/10.1016/j.ppnp.2020.103775)
- [61] L. W. Chen, C. M. Ko and B. A. Li, Light cluster production in intermediate-energy heavy ion collisions induced by neutron rich nuclei, Nucl. Phys. A **729**, 809-834 (2003). doi: [10.1016/j.nuclphysa.2003.09.010](https://doi.org/10.1016/j.nuclphysa.2003.09.010)
- [62] Y. Wang, C. Guo, Q. Li et al., $^3\text{H}/^3\text{He}$ ratio as a probe of the nuclear symmetry energy at sub-saturation densities, Eur. Phys. J. A **51**, 37 (2015). doi: [10.1140/epja/i2015-15037-8](https://doi.org/10.1140/epja/i2015-15037-8)
- [63] T. Gaitanos, M. Colonna, M. Di et al., Stopping and isospin equilibration in heavy ion collisions, Phys. Lett. B **595**, 209-215 (2004). doi: [10.1016/j.physletb.2004.05.080](https://doi.org/10.1016/j.physletb.2004.05.080)
- [64] G. C. Yong, B. A. Li, L. W. Chen et al., Triton-He-3 relative and differential flows as probes of the nuclear symmetry energy at supra-saturation densities, Phys. Rev. C **80**, 044608 (2009). doi: [10.1103/PhysRevC.80.044608](https://doi.org/10.1103/PhysRevC.80.044608)
- [65] P. Chomaz and F. Gulminelli, Phase transition in an isospin dependent lattice gas model, Phys. Lett. B **447**, 221-226 (1999). doi: [10.1016/S0370-2693\(99\)00003-9](https://doi.org/10.1016/S0370-2693(99)00003-9)
- [66] S. Albergo, S. Costa, E. Costanzo et al., Temperature and free-nucleon densities of nuclear matter exploding into light clusters in heavy-ion collisions Nuovo Cim. A **89**, 1-28 (1985). doi: [10.1007/BF02773614](https://doi.org/10.1007/BF02773614)
- [67] H. S. Xu, M. B. Tsang, T. X. Liu et al., Isospin fractionation in nuclear multifragmentation, Phys. Rev. Lett. **85**, 716-719 (2000). doi: [10.1103/PhysRevLett.85.716](https://doi.org/10.1103/PhysRevLett.85.716)

- 723 [68] M. A. Famiano, T. Liu, W. G. Lynch et al., Neutron and Pro-
724 ton Transverse Emission Ratio Measurements and the Den-
725 sity Dependence of the Asymmetry Term of the Nuclear
726 Equation of State, Phys. Rev. Lett. **97**, 052701 (2006). doi:
727 [10.1103/PhysRevLett.97.052701](https://doi.org/10.1103/PhysRevLett.97.052701)
- 728 [69] S. Nagamiya, M. C. Lemaire, E. Moller, Production of Pi-
729 ons and Light Fragments at Large Angles in High-Energy
730 Nuclear Collisions, Phys. Rev. C **24**, 971-1009 (1981). doi:
731 [10.1103/PhysRevC.24.971](https://doi.org/10.1103/PhysRevC.24.971)
- 732 [70] M. Veselsky, R. W. Ibbotson, R. Laforest et al., Isospin de-
733 pendence of isobaric ratio $Y(^3H) / Y(^3He)$ and its possible
734 statistical interpretation, Phys. Lett. B **497**, 1-7 (2001). doi:
735 [10.1016/S0370-2693\(00\)01318-6](https://doi.org/10.1016/S0370-2693(00)01318-6)
- 736 [71] F. Rami et al.,[FOPI], Isospin tracing: A Probe of nonequi-
737 librium in central heavy ion collisions, Phys. Rev. Lett. **84**,
738 1120-1123 (2000). doi: [10.1103/PhysRevLett.84.1120](https://doi.org/10.1103/PhysRevLett.84.1120)
- 739 [72] Y. B. Gurov, L. Y. Korotkova, S. V. Lapushkin et al., Yields
740 of triton and 3He produced by nuclei in reactions of stopped
741 pion absorption, Bull. Russ. Acad. Sci. Phys. **78**, 1112-1116
742 (2014). doi: [10.3103/S1062873814110100](https://doi.org/10.3103/S1062873814110100)
- 743 [73] G. Poggi, G. Pasquali, M. Bini et al., Evidence for collective
744 expansion in light-particle emission following Au+Au colli-
745 sions at 100, 150 and 250 A-MeV, Nucl. Phys. A **586**, 755-776
746 (1995). doi: [10.1016/0375-9474\(95\)00042-Y](https://doi.org/10.1016/0375-9474(95)00042-Y)
- 747 [74] R. Bougault, P. Eudes, D. Gourio et al., A possible scenario
748 for the time dependence of the multifragmentation process in
749 $Xe + Sn$ collisions: an explanation of the 3He puzzle. No.
750 DAPNIA-SPHN-97-024. SCAN-9709121, (1997).
- 751 [75] T. X. Liu, W. G. Lynch, R. H. Showalter et al., Isospin observ-
752 ables from fragment energy spectra, Phys. Rev. C **86**, 024605
753 (2012). doi: [10.1103/PhysRevC.86.024605](https://doi.org/10.1103/PhysRevC.86.024605)
- 754 [76] M. A. Lisa et al.,[EOS], Radial flow in Au + Au collisions at E
755 = 0.25-A/GeV - 1.15-A/GeV, Phys. Rev. Lett. **75**, 2662-2665
756 (1995). doi: [10.1103/PhysRevLett.75.2662](https://doi.org/10.1103/PhysRevLett.75.2662)
- 757 [77] A. Bonasera, M. Bruno, C. Dorso et al., Critical phenomena in
758 nuclear fragmentation, Rivista del Nuovo Cimento, 23:1-101,
759 (2000). doi: [10.1007/BF03548882](https://doi.org/10.1007/BF03548882)
- 760 [78] W. Neubert and A. S. Botvina, What is the physics behind the
761 3He - 4He anomaly?, Eur. Phys. J. A **7**, 101-106 (2000). doi:
762 [10.1007/s100500050016](https://doi.org/10.1007/s100500050016)
- 763 [79] D. V. Shetty, A. Keksis, E. Martin et al., Intermediate mass
764 fragments and isospin dependence in ^{124}Sn , $^{124}Xe + ^{124}Sn$,
765 ^{112}Sn reactions at 28-MeV/nucleon, Phys. Rev. C **68**, 054605
766 (2003). doi: [10.1103/PhysRevC.68.054605](https://doi.org/10.1103/PhysRevC.68.054605)
- 767 [80] S. Piantelli, G. Casini, A. Ono et al., Isospin transport phe-
768 nomena for the systems $^{80}Kr + ^{40,48}Ca$ at 35 MeV/nucleon,
769 Phys. Rev. C **103**, 014603 (2021). doi: [10.1103/Phys-](https://doi.org/10.1103/Phys-)
770 [RevC.103.014603](https://doi.org/10.1103/PhysRevC.103.014603)
- 771 [81] W. Reisdorf et al.,[FOPI], Systematics of central heavy ion
772 collisions in the 1A GeV regime, Nucl. Phys. A **848**, 366-427
773 (2010). doi: [10.1016/j.nuclphysa.2010.09.008](https://doi.org/10.1016/j.nuclphysa.2010.09.008)
- 774 [82] F. Guan, X. Diao, Y. Wang et al., A Compact Spec-
775 tometer for Heavy Ion Experiments in the Fermi energy
776 regime, Nucl. Instrum. Meth. A **1011**, 165592 (2021). doi:
777 [10.1016/j.nima.2021.165592](https://doi.org/10.1016/j.nima.2021.165592)
- 778 [83] Y. J. Wang, F. H. Guan, X. Y. Diao et al., CSHINE for studies
779 of HBT correlation in Heavy Ion Reactions, Nucl. Sci. Tech.
780 **32**, 4 (2021). doi: [10.1007/s41365-020-00842-2](https://doi.org/10.1007/s41365-020-00842-2)
- 781 [84] Z. Sun, W.L. Zhan, Z.Y. Guo et al., RIBLL, the radioactive ion
782 beam line in Lanzhou, Nucl. Instrum. Meth. A **503**, 496-503
783 (2003).. doi: [10.1016/S0168-9002\(03\)01005-2](https://doi.org/10.1016/S0168-9002(03)01005-2)
- 784 [85] J. W. Xia, W. L. Zhan, B. W. Wei et al., The heavy ion
785 cooler-storage-ring project (HIRFL-CSR) at Lanzhou, Nucl.
786 Instrum. Meth. A **488**, 11-25 (2002). doi: [10.1016/S0168-9002\(02\)00475-8](https://doi.org/10.1016/S0168-9002(02)00475-8)
- 787 [86] F. Guan, Y. Wang, X. Diao et al., Track recogni-
788 tion for the $\Delta E-E$ telescopes with silicon strip detec-
789 tors, Nucl. Instrum. Meth. A **1029**, 166461 (2022). doi:
790 [10.1016/j.nima.2022.166461](https://doi.org/10.1016/j.nima.2022.166461)
- 791 [87] X. Y. Diao, F. H. Guan, Y. J. Wang et al., Reconstruction of
792 fission events in heavy ion reactions with the compact spec-
793 trometer for heavy ion experiment, Nucl. Sci. Tech. **33**, 40
794 (2022). doi: [10.1007/s41365-022-01024-y](https://doi.org/10.1007/s41365-022-01024-y)
- 795 [88] X. Wei, F. Guan, H. Yang et al., Development of Parallel
796 Plate Avalanche Counter for heavy ion collision in radioac-
797 tive ion beam, Nucl. Eng. Tech. **52**, 575-580 (2020). doi:
798 [10.1016/j.net.2019.08.020](https://doi.org/10.1016/j.net.2019.08.020)
- 799 [89] D. Guo, Y. Qin, S. Xiao et al., An FPGA-based trigger
800 system for CSHINE, Nucl. Sci. Tech. **33**, 162 (2022). doi:
801 [10.1007/s41365-022-01149-0](https://doi.org/10.1007/s41365-022-01149-0)
- 802 [90] Y. Zhang, N. Wang, Q. F. Li et al., Progress of quan-
803 tum molecular dynamics model and its applications in heavy
804 ion collisions, Front. Phys. (Beijing) **15**, 54301 (2020). doi:
805 [10.1007/s11467-020-0961-9](https://doi.org/10.1007/s11467-020-0961-9)
- 806 [91] R. J. Charity, M. A. McMahan, G. J. Wozniak et al., System-
807 atics of complex fragment emission in niobium-induced reac-
808 tions, Nucl. Phys. A **483**, 371-405 (1988). doi: [10.1016/0375-9474\(88\)90542-8](https://doi.org/10.1016/0375-9474(88)90542-8)
- 809 [92] R. J. Charity, L. G. Sobotka, J. Cibor et al., Emission of unsta-
810 ble clusters from hot Yb compound nuclei, Phys. Rev. C **63**,
811 024611 (2001). doi: [10.1103/PhysRevC.63.024611](https://doi.org/10.1103/PhysRevC.63.024611)
- 812 [93] J. Aichelin, C. Hartnack, A. Bohne et al., QMD versus
813 BUU/VUU: Same results from different theories, Phys. Lett.
814 B **224**, 34-39 (1989). doi: [10.1016/0370-2693\(89\)91045-9](https://doi.org/10.1016/0370-2693(89)91045-9)
- 815 [94] J. Aichelin, 'Quantum' molecular dynamics: A Dynamical
816 microscopic n body approach to investigate fragment forma-
817 tion and the nuclear equation of state in heavy ion colli-
818 sions, Phys. Rept. **202**, 233-360 (1991). doi: [10.1016/0370-1573\(91\)90094-3](https://doi.org/10.1016/0370-1573(91)90094-3)
- 819 [95] R. S. Wang, L. Ou and Z. G. Xiao, Production of high-energy
820 neutron beam from deuteron breakup, Nucl. Sci. Tech. **33**, 92
821 (2022). doi: [10.1007/s41365-022-01075-1](https://doi.org/10.1007/s41365-022-01075-1)
- 822 [96] L. Ou and Z. G. Xiao, Orientation dichroism effect of pro-
823 ton scattering on deformed nuclei, Chin. Phys. C **44**, 114103
824 (2020). doi: [10.1088/1674-1137/abaf1](https://doi.org/10.1088/1674-1137/abaf1)
- 825 [97] X. Liang, L. Ou and Z. Xiao, New probe to study the
826 symmetry energy at low nuclear density with the deuteron
827 breakup reaction, Phys. Rev. C **101**, 024603 (2020). doi:
828 [10.1103/PhysRevC.101.024603](https://doi.org/10.1103/PhysRevC.101.024603)
- 829 [98] L. W. Chen, C. M. Ko, B. A. Li et al., Density slope of
830 the nuclear symmetry energy from the neutron skin thick-
831 ness of heavy nuclei, Phys. Rev. C **82**, 024321 (2010). doi:
832 [10.1103/PhysRevC.82.024321](https://doi.org/10.1103/PhysRevC.82.024321)
- 833 [99] Y. Zhang, Z. Li, C. Zhou et al., Effect of isospin depen-
834 dent cluster recognition on the observables in heavy ion col-
835 lisions, Phys. Rev. C **85**, 051602 (2012). doi: [10.1103/Phys-](https://doi.org/10.1103/Phys-)
836 [RevC.85.051602](https://doi.org/10.1103/PhysRevC.85.051602)
- 837 [100] J. Zheng, E. Wu, C. Zhang et al., Measurement of Fission
838 Time Scale and Excitation Energy at Scission for 25MeV/u
839 $^{40}Ar + ^{209}Bi$ Fission Reaction, Chinese Physics C, 23, 946-953
840 (1999).
- 841 [101] H. H. Gutbrod, A. Sandoval, P. J. Johansen et al., Final State
842 Interactions in the Production of Hydrogen and Helium Iso-
843 topes by Relativistic Heavy Ions on Uranium, Phys. Rev. Lett.
844 **37**, 667-670 (1976). doi: [10.1103/PhysRevLett.37.667](https://doi.org/10.1103/PhysRevLett.37.667)

- 848 [102] W. Reisdorf et al.,[FOPI], Central collisions of Au on Au at 884 RevC.[98.044611](#)
 849 150, 250 and 400 MeV/nucleon, Nucl. Phys. A **612**, 493-556
 850 (1997). doi: [10.1016/S0375-9474\(96\)00388-0](#)
- 851 [103] H. Xi, M. J. Huang, W. G. Lynch et al., Examining the cool- 885 E. Plagnol, J. Lukasik, G. Auger et al., Onset of midvelocity
 852 ing of hot nuclei, Phys. Rev. C **57**, R462-R465 (1998). doi: 886 emissions in symmetric heavy ion reactions, Phys. Rev. C **61**,
 853 [10.1103/PhysRevC.57.R462](#) 014606 (2000). doi: [10.1103/PhysRevC.61.014606](#)
- 854 [104] A. R. Raduta, E. Bonnet, B. Borderie et al., Break-up stage 887 S. Piantelli, L. Bidini, G. Poggi et al., Intermediate Mass Frag-
 855 restoration in multifragmentation reactions, Eur. Phys. J. A **32**, 888 ment Emission Pattern in Peripheral Heavy-Ion Collisions
 856 175-182 (2007). doi: [10.1140/epja/i2006-10381-4](#) at Fermi Energies, Phys. Rev. Lett. **88**, 052701 (2002). doi:
 857 [105] L. G. Sobotka, Simulations of collisions between nuclei at 889 [10.1103/PhysRevLett.88.052701](#)
- 858 intermediate energy using the Boltzmann-Uehling-Uhlenbeck 890 D. Theriault, J. Gauthier, F. Grenier et al., Neutron to proton
 859 equation with neutron skin producing potentials, Phys. Rev. C **50**, 891 ratios of quasiprojectile and midrapidity emission in the ^{64}Zn
 860 R1272-R1275 (1994). doi: [10.1103/PhysRevC.50.R1272](#) + ^{64}Zn reaction at 45-MeV/nucleon, Phys. Rev. C **74**, 051602
 861 [106] R. Lonti, V. Baran, M. Colonna et al., Isospin dynamics in 892 (2006). doi: [10.1103/PhysRevC.74.051602](#)
- 862 fragmentation reactions at Fermi energies, Phys. Lett. B **625**, 893 R. Planeta et al.,[ISOSPIN], Centrality dependence of isospin
 863 33 (2005). doi: [10.1016/j.physletb.2005.08.044](#) effect signatures in $^{124}\text{Sn} + ^{64}\text{Ni}$ and $^{112}\text{Sn} + ^{58}\text{Ni}$ reac-
 864 [107] V. Baran, M. Colonna, V. Greco et al., Reaction dynamics 894 tions, Phys. Rev. C **77**, 014610 (2008). doi: [10.1103/Phys-
 865 with exotic beams, Phys. Rept. **410**, 335-466 \(2005\). doi: 895 RevC.77.014610](#)
- 866 [10.1016/j.physrep.2004.12.004](#)
- 867 [108] D. D. S. Coupland, W. G. Lynch, M. B. Tsang et al., Influence 896 Z. Kohley, L. W. May, S. Wuenschel et al., Transverse collec-
 868 of Transport Variables on Isospin Transport Ratios, Phys. Rev. 897 tive flow and midrapidity emission of isotopically identified
 869 C **84**, 054603 (2011). doi: [10.1103/PhysRevC.84.054603](#) light charged particles, Phys. Rev. C **83**, 044601 (2011). doi:
 870 [109] V. Baran, M. Colonna, M. Di Toro et al., From multifragmen- 898 [10.1103/PhysRevC.83.044601](#)
- 871 tation to neck fragmentation: Mass, isospin, and velocity cor- 899 R. Ogul, A. S. Botvina, M. Bleicher et al., Isospin com-
 872 relations, Phys. Rev. C **85**, 054611 (2012). doi: [10.1103/Phys- 900 positions of correlated sources in the Fermi energy do-
 873 RevC.85.054611](#) main, Phys. Rev. C **107**, 054606 (2023). doi: [10.1103/Phys-
 874 \[110\] L. G. Sobotka, R. J. Charity, D. K. Agnihotri et al., 901 RevC.107.054606](#)
- 875 Neutron-proton asymmetry of the midvelocity material in an 902 Y. Qin, Q. Niu, D. Guo et al., Probing high-momentum com-
 876 intermediate-energy heavy ion collision, Phys. Rev. C **62**, 903 ponent in nucleon momentum distribution by neutron-proton
 877 031603 (2000). doi: [10.1103/PhysRevC.62.031603](#) bremsstrahlung γ -rays in heavy ion reactions, Phys. Lett. B **850**, 138514 (2024). doi: [10.1016/j.physletb.2024.138514](#)
- 878 [111] S. Piantelli, P. R. Maurenzig, A. Olmi et al., Distinctive 904 R. Wang, Y. G. Ma, L. W. Chen et al., Kinetic approach
 879 features of Coulomb-related emissions in peripheral heavy ion 905 of light-nuclei production in intermediate-energy heavy-
 880 collisions at Fermi energies, Phys. Rev. C **76**, 061601 (2007). 906 ion collisions, Phys. Rev. C **108**, L031601 (2023). doi:
 881 doi: [10.1103/PhysRevC.76.061601](#) [10.1103/PhysRevC.108.L031601](#)
- 882 [112] E. Vient et al.,[INDRA], New “3D calorimetry” of hot nu- 907 K. Pomorski, B. Nerlo-Pomorska, A. Surowiec et al., Light
 883 clei, Phys. Rev. C **98**, 044611 (2018). doi: [10.1103/Phys- 908 particle emission from the fissioning nuclei Ba-126, Pt-188
 884 RevC.98.044611](#) and 110-266, 110-272, 110-278: Theoretical predictions and
 885 experimental results, Nucl. Phys. A **679**, 25-53 (2000). doi:
 886 [10.1016/S0375-9474\(00\)00327-4](#) [10.1103/PhysRevC.61.014606](#)